Entanglement-Optimal Trajectories of Many-Body Quantum Markov Processes

Tatiana Vovk and Hannes Pichler*
Institute for Theoretical Physics, University of Innsbruck, 6020 Innsbruck, Austria
and Institute for Quantum Optics and Quantum Information of the Austrian Academy of Sciences, 6020 Innsbruck, Austria

(Received 24 November 2021; accepted 13 May 2022; published 13 June 2022)

We develop a novel approach aimed at solving the equations of motion of open quantum many-body systems. It is based on a combination of generalized wave function trajectories and matrix product states. We introduce an adaptive quantum stochastic propagator, which minimizes the expected entanglement in the many-body quantum state, thus minimizing the computational cost of the matrix product state representation of each trajectory. We illustrate this approach on the example of a one-dimensional open Brownian circuit. We show that this model displays an entanglement phase transition between area and volume law when changing between different propagators and that our method autonomously finds an efficiently representable area law unraveling.

DOI: 10.1103/PhysRevLett.128.243601

Classical simulation of the evolution of quantum many-body systems is a formidably hard task, in particular if the system is fully coherent [1]. Most near-term intermediate scale quantum devices are, however, noisy, which opens a possibility for the existence of efficient classical algorithms for simulating the corresponding open system dynamics. Nonetheless it is often unclear how to best exploit this potential.

Here we address this challenge by developing an algorithm that explicitly harnesses the quantum noise inherent to an open quantum system to minimize the computational cost of representing the many-body state. Our approach is based on a combination of matrix product states (MPSs) [2–4] and a generalization of the quantum trajectory (QT) method [5–10]. The latter identifies the dynamics of an open quantum system as a stochastic evolution of pure quantum states, corresponding to a continuous measurement of the environment [11]. Importantly, the choice of the monitored environment observables results in qualitatively different ensembles of QTs. Our method utilizes this flexibility and continuously optimizes the monitored environment observables by predicting and minimizing the expected entanglement in the trajectory wave function (Fig. 1), thus minimizing the computational cost of MPS representations.

We illustrate our approach by applying it to solve the Markovian master equation (ME) of an open Brownian circuit, where the coherent part of the evolution rapidly generates entanglement, while the dissipative part leads to dephasing. We show that various types of QT methods lead to ensembles that differ dramatically in their entanglement properties. This includes a phase transition between area law and volume law entangled ensembles, depending on the monitored environment observables. In addition to being an interesting phenomenon *per se*, with connections to recently discussed measurement-induced phase transitions [12–23], it provides an ideal test bed for our algorithm: We show that our entanglement predictor allows one to generate ensembles of QTs that keep the system in the area-law phase at all times.

We are interested in open quantum many-body systems with n constituents and m dissipative channels described by a ME of a generic Lindblad form ($\hbar = 1$) [24]:

$$\frac{d\rho}{dt} = -i[H_{\mathrm{sys}}, \rho] + \sum_{j=1}^{m} \gamma_j \left(c_j \rho c_j^\dagger - \frac{1}{2}\{\rho, c_j^\dagger c_j\} \right). \quad (1)$$

Here, ρ is the (many-body) density operator of the quantum system, H_{sys} is the (so far unspecified, potentially time-dependent) system Hamiltonian, and the c_j's are the jump operators corresponding to the jth decay channel with

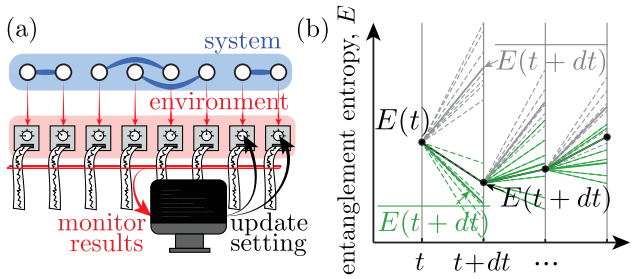

FIG. 1. (a) Schematic setting of a continuously monitored quantum many-body system with adaptive measurements. (b) Propagation of a state from time t into the future with two options for the stochastic propagator (color coded, gray vs green). The colored dashed lines are potential QTs for a given unraveling, and their stochastic averages are shown as solid lines. A QT (black) is generated randomly at each time step, corresponding to the stochastic propagator that gives the lowest expected entanglement (green).

associated decay rate γ_j. In the following it is convenient to assume that $H_{\rm sys}$ is short-range interacting and the jump operators are local. Such a ME describes the reduced dynamics of a system coupled to an environment (or bath). The underlying joint evolution of system and environment is unitary and is described by the Schrödinger equation $i\partial_t|\Psi(t)\rangle = H(t)|\Psi(t)\rangle$, where $|\Psi(t)\rangle$ represents the joint state of the system and environment, and the Hamiltonian is given by [11]

$$H(t) = H_{\rm sys} + i\sum_{j=1}^{m}\sqrt{\gamma_j}\,[b_j(t)^\dagger c_j - c_j^\dagger b_j(t)]. \quad (2)$$

Here, $b_j(t)$'s are so-called quantum noise operators with bosonic statistics $[b_j(t), b_{j'}(t')^\dagger] = \delta_{j,j'}\delta(t-t')$. Those operators act on the degrees of freedom of the environment, which are initially in the vacuum state: $b_j(t)|\Psi(0)\rangle = 0$. The ME [Eq. (1)] is obtained from the full Schrödinger equation by tracing out these bosonic degrees of freedom [11].

The QT method solves the ME [Eq. (1)] by simulating a continuous monitoring of the environmental degrees of freedom in Eq. (2). It stochastically generates an ensemble of pure states of the system, called *quantum trajectories*, from which the density matrix dynamics can be retrieved as a statistical average:

$$\rho(t) = \lim_{N\to\infty}\frac{1}{N}\sum_{k=1}^{N}|\phi^{(k)}(t)\rangle\langle\phi^{(k)}(t)|. \quad (3)$$

Here the quantum trajectories $|\phi^{(k)}(t)\rangle$ represent the conditional state of the system for a particular (simulated) measurement history of the monitored environment (enumerated by k). They satisfy a stochastic equation of motion, i.e., a quantum stochastic Schrödinger equation (QSSE) [11]. The form of the QSSE depends on the environment monitoring schemes, in particular on the monitored observables. For instance, the standard QT method, known as quantum jump approach, is obtained by continuous monitoring of the photon numbers $b_j^\dagger(t)b_j(t)$ [5–7,9]. Another approach is based on the balanced homodyne measurement, where a phase-sensitive homodyne current $b_j(t)e^{i\varphi_j} + b_j^\dagger(t)e^{-i\varphi_j}$ is continuously measured [8]. Here, the φ_j specifies the measured quadrature.

A QT is generated by integrating the QSSE in (small) time steps, dt. In practice, one Trotterizes the corresponding propagator into a stochastic and a deterministic part. The stochastic component can be further split into independent components corresponding to m decay channels [25]. Specifically, a single integration step $|\phi^{(k)}(t)\rangle \to |\phi^{(k)}(t+dt)\rangle$ is achieved by a sequential application of stochastic operators K_j for each decay channel j: Starting from the state $|\phi_1^{(k)}(t)\rangle = |\phi^{(k)}(t)\rangle$, one generates the sequence of normalized states

$$|\phi_{j+1}^{(k)}(t)\rangle \propto K_j|\phi_j^{(k)}(t)\rangle, \qquad (j=1,\ldots,m) \quad (4)$$

and then concludes the integration step with the unitary operation $|\phi^{(k)}(t+dt)\rangle = e^{-iH_{\rm sys}dt}|\phi_{m+1}^{(k)}(t)\rangle$. The form of the stochastic operator K_j depends on the type of (simulated) environment measurement. For example, the operator simulating a homodyne measurement of the output field in channel j is

$$K_j^{\rm hom} = e^{-\gamma_j dt c_j^\dagger c_j/2} + \sqrt{\gamma_j}c_j e^{i\varphi_j}d\xi_j(t), \quad (5)$$

where $d\xi_j(t) = \sqrt{\gamma_j}\langle\phi_j^{(k)}(t)|c_j e^{i\varphi_j} + c_j^\dagger e^{-i\varphi_j}|\phi_j^{(k)}(t)\rangle dt + dW_j(t)$ and the $dW_j(t)$'s are independent, normally distributed Gaussian variables with zero mean and variance dt, also known as Wiener increments. For a simulated number measurement, the propagator is probabilistically selected from the two options:

$$K_j^{\rm num} = \begin{cases}\sqrt{\gamma_j dt}c_j & \text{with probability } p_j,\\ e^{-\gamma_j dt c_j^\dagger c_j/2} & \text{with probability } 1-p_j,\end{cases} \quad (6)$$

where $p_j = \gamma_j dt\langle\phi_j^{(k)}(t)|c_j^\dagger c_j|\phi_j^{(k)}(t)\rangle$ corresponds to the probability of measuring a photon in channel j between t and $t+dt$.

While these two schemes are by far the most common ones, we stress that a multitude of stochastic propagators can be constructed by choosing different measurements of the bath operators specified via the eigenbases of arbitrary Hermitian functions of the bath operators, $X_j(t) = f[b_j(t), b_j^\dagger(t)]$. This also includes measurement strategies that change with time and depend on prior measurement outcomes [26,27]. Importantly, the stochastic averages over linear functionals of the state projectors $\phi^{(k)} = |\phi^{(k)}\rangle\langle\phi^{(k)}|$ do not depend on how the environment is monitored. This includes in particular the density operator [Eq. (3)] and the expectation values of linear observables. However the ensemble of QTs itself, as well as nonlinear functionals of the trajectories, *does depend* on the unraveling. In particular this holds for the entanglement entropy (EE), which is of central interest in our work. We consider the EE between two partitions of the many-body system, $A \cup B$. In this case the EE of a single QT $|\phi^{(k)}\rangle$ is defined as the von Neumann entropy of the reduced state of one of the subsystems $\{\rho_A^{(k)} = {\rm tr}_B[\phi^{(k)}]\}$:

$$E[\phi^{(k)}] = S[\rho_A^{(k)}] = -{\rm tr}[\rho_A^{(k)}\log_2\rho_A^{(k)}]. \quad (7)$$

The ensemble averaged EE (EAEE) is then defined as

$$\bar{E} = \lim_{N\to\infty}\frac{1}{N}\sum_{k=1}^{N}E[\phi^{(k)}]. \quad (8)$$

It is bounded from below by the entanglement of formation [28] of the density operator $E_f(\rho)$ and from above by the entropies of $\rho_A = {\rm tr}_B(\rho)$ and $\rho_B = {\rm tr}_A(\rho)$:

$$E_f(\rho) \leq \bar{E} \leq \min\left[S(\rho_A), S(\rho_B)\right]. \tag{9}$$

The dependence of the EAEE on the unraveling becomes especially important when the QT method is combined with MPS techniques to represent and propagate the (stochastic) wave function of the quantum many-body system. MPS representations are efficient as long as the bond dimension χ, and thus the entanglement, is small. Since the computational cost of a MPS simulation grows exponentially with the entanglement, choosing the unraveling that minimizes the EAEE is of paramount importance. *A priori* it is unclear which stochastic propagation scheme leads to small values of the EAEE, without constructing the trajectories [29]. We can however predict how various types of the stochastic propagators affect the change rate of the EAEE at each instant of time and accordingly optimize it. This motivates a time-local greedy algorithm that continuously adapts the stochastic propagators to the conditional wave function as time progresses [Fig. 1(a)].

More specifically, given the pure state of the system $|\phi^{(k)}(t)\rangle$ of the kth trajectory at time t, we want to choose the stochastic propagator that minimizes the expected instantaneous entanglement increase rate, $\dot{\bar{E}} = d\bar{E}/dt$ [see Fig. 1(b)]. For simplicity we consider only propagators corresponding to independent measurements of each bath channel j and jump operators that do not couple the partitions A and B. As outlined above, the stochastic components of the propagator can then be applied in sequences. This allows one to optimize the corresponding change rate of the EAEE, $\dot{\bar{E}}_j$, channel by channel. Remarkably, one can analytically perform the minimization $\min_{X_j(t)}(\dot{\bar{E}}_j)$ over all stochastic propagators that correspond to measurements in eigenbases of arbitrary bath observables $X_j(t) = f[b_j(t), b_j^\dagger(t)]$. Moreover, the minimum is always obtained either for a number measurement, $X_j(t) = b_j^\dagger(t)b_j(t)$, or for a homodyne measurement, $X_j(t) = b_j(t)e^{i\varphi_j} + b_j^\dagger(t)e^{-i\varphi_j}$. For the number measurement the EAEE change rate at channel j is

$$\dot{\bar{E}}_j^{\text{num}} = \mathrm{tr}(c_j\phi c_j^\dagger)\log_2\left[\mathrm{tr}(c_j\phi c_j^\dagger)\right] + \mathrm{tr}(\mathrm{tr}_B(c_j\phi c_j^\dagger)\{\log_2\left[\mathrm{tr}_B(\phi)\right] - \log_2\left[\mathrm{tr}_B(c_j\phi c_j^\dagger)\right]\}). \tag{10}$$

The measurement of the homodyne current gives instead

$$\dot{\bar{E}}_j^{\text{hom}} = \frac{1}{2\ln 2}\Bigg[|e^{-i\varphi_j}\mathrm{tr}(c_j\phi) + e^{i\varphi_j}\mathrm{tr}(\phi c_j^\dagger)|^2 - \sum_{k,\ell}\frac{\ln(\xi_k) - \ln(\xi_\ell)}{\xi_k - \xi_\ell}|e^{-i\varphi_j}\langle\xi_k|\mathrm{tr}_B(c_j\phi)|\xi_\ell\rangle + e^{i\varphi_j}\langle\xi_k|\mathrm{tr}_B(\phi c_j^\dagger)|\xi_\ell\rangle|^2\Bigg]. \tag{11}$$

Here $\phi = |\phi_j^{(k)}(t)\rangle\langle\phi_j^{(k)}(t)|$ [see Eq. (4)] and $\mathrm{tr}_B(\phi)|\xi_\ell\rangle = \xi_\ell|\xi_\ell\rangle$. We refer the reader to the Supplemental Material, Sec. III [26], for the proof and derivation of the above statements.

This motivates the following entanglement-optimized quantum trajectory (EOQT) algorithm [see Fig. 2(a)]. For each discrete time step dt propagate the state $|\phi^{(k)}(t)\rangle \to |\phi^{(k)}(t+dt)\rangle$ as follows: (1) Sequentially for each channel j calculate the EAEE change rates $\min_{\varphi_j}\dot{\bar{E}}_j^{\text{hom}}$ and $\dot{\bar{E}}_j^{\text{num}}$ and update the state according to the correspondingly optimal stochastic propagator; (2) Complete the update of the resulting state by applying the coherent propagator $e^{-iH_{\text{sys}}dt}$.

This EOQT algorithm can be naturally combined with MPS methods, such as the time evolving block decimation (TEBD) algorithm [30,31] [see Fig. 2(a)]. Importantly, the computational cost of the evaluation and optimization of Eqs. (10) and (11) for a MPS with bond dimension χ is $\mathcal{O}(\chi^3 d)$, where d is the local Hilbert space dimension. This should be compared with the cost of the coherent propagation, which for each of the time steps dt is $\mathcal{O}(\chi^3 d^3 n)$. Thus the EAEE optimization does not significantly add to the cost of the standard propagation. On the other hand, the potential gain in the simulation efficiency can be substantial, as we show in the remainder of this Letter.

The simplest example illustrating the dependence of $\bar{E}$ on the unraveling is obtained by considering two qubits initially in a Bell state, $(|00\rangle + |11\rangle)/\sqrt{2}$, that are undriven ($H_{\text{sys}} = 0$) and coupled to a bath with a jump operator $c_j = |1\rangle_j\langle 1|$ and strength $\gamma_j = \gamma$ ($j = 1, 2$). In this case, $\bar{E}$ can be analytically calculated for different unravelings. For the photon number measurements, one obtains $\bar{E}^{\text{num}} = \sigma(2\gamma t)$, where we introduced the function

$$\sigma(s) = \frac{1}{2\ln 2}\left[(1 + e^{-s})\ln(1 + e^{-s}) + se^{-s}\right]. \tag{12}$$

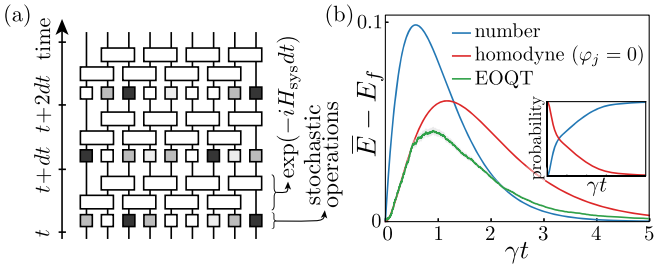

FIG. 2. (a) Schematic illustration of the EOQT-MPS algorithm. To propagate a state from t to $t + dt$ we first apply a "stochastic layer": We calculate the unraveling that minimizes the expected EE in the next time step and apply the corresponding stochastic propagator. This procedure is implemented sequentially for all jump operators. Then we implement a "deterministic layer," propagating the system with H_{sys} via standard methods such as TEBD. (b) Time dependence of the excess EAEE, $\bar{E} - E_f$, of a continuously monitored Bell pair for the number measurement (blue), the homodyne unraveling with $\varphi_j = 0$ (red), and the EOQT (green, number of trajectories $N = 10^4$). Inset: The statistics of measurement choices of the EOQT algorithm. The error bars are denoted by gray filling.

The expression for homodyne measurement is

$$\bar{E}^{\mathrm{hom}}(\tau) = \frac{1}{2\sqrt{2\pi\tau}} \int ds \sigma(s) e^{-\frac{(s-2\tau)^2}{8\tau}} \tag{13}$$

with $\tau = \gamma t(\cos^2\varphi_1 + \cos^2\varphi_2)$. In Fig. 2 we compare the excess entanglements $\bar{E} - E_f$ for number, homodyne, and optimal (EOQT) measurements. In this case E_f evaluates to $E_f(t) = -r_+ \log_2(r_+) - r_- \log_2(r_-)$, where $r_\pm = (1 \pm \sqrt{1 - e^{-2\gamma t}})/2$ [28]. We note that for short times the homodyne unraveling with $\varphi_j = 0$ $(j = 1, 2)$ saturates this bound, while for longer times the number unraveling approaches E_f faster [Fig. 2(b)]. The optimized algorithm indeed finds unravelings resulting in an EAEE that is always close to the theoretical minimum E_f. As visible in the inset of Fig. 2(b), the optimizer chooses mostly the homodyne propagator with $\varphi_j = 0$ for early times and switches over to predominantly choosing the number propagators around $\gamma t \approx 1$.

To demonstrate the potential of our approach in a many-body setting, we consider a one-dimensional open random Brownian circuit (RBC) for a chain of spin-1/2 particles. We choose this example since the evolution under the RBC leads to rapid EE growth. The coherent part of the evolution is given by the time-dependent RBC Hamiltonian:

$$H_{\mathrm{sys}}(t) = \sum_{j=1}^{n-1} \sum_{k,\ell=0}^{3} g_j^{k,\ell}(t) \sigma_j^k \otimes \sigma_{j+1}^{\ell}. \tag{14}$$

Here n is the number of spins and $\sigma_j^k \in \{\mathbb{1}_j, \sigma_j^x, \sigma_j^y, \sigma_j^z\}$ are standard Pauli operators acting on spin j. The parameters $g_j^{k,\ell}(t)$ are Gaussian stochastic variables with $\langle\langle g_j^{k,\ell}(t) \rangle\rangle = 0$ and $\langle\langle g_j^{k,\ell}(t) g_{j'}^{k',\ell'}(t') \rangle\rangle = \alpha \delta_{j,j'} \delta_{k,k'} \delta_{\ell,\ell'} \delta(t - t')$, where $\langle\langle \cdots \rangle\rangle$ denotes the average over Hamiltonian realizations and α is the variance of RBC. The incoherent part is given by the jump operators $c_j = \sigma_j^z$ with uniform decay strength (measurement rate), $\gamma_j = \gamma$.

For sufficiently strong γ this model exhibits a type of measurement-induced phase transition that is *solely* driven by the type of unraveling (see Fig. 3). Depending on the bath measurement operators, the character of EAEE changes from area law to volume law. That is, even though all types of bath measurements solve in the end the same ME [Eq. (1)], some unravelings lead to ensembles with area law EAEE that can be efficiently computed on classical computers, while other unravelings fail to do so.

This change from volume to area law can be shown explicitly by considering the stochastic propagator for a homodyne unraveling K_j, defined above [see Eq. (5)]. Since $\sigma_j^{z\dagger}\sigma_j^z = \sigma_j^{z2} = \mathbb{1}$, it takes the form

$$K_j \propto \exp\{e^{i\varphi_j}\sqrt{\gamma}\sigma_j^z d\xi_j(t)\}, \tag{15}$$

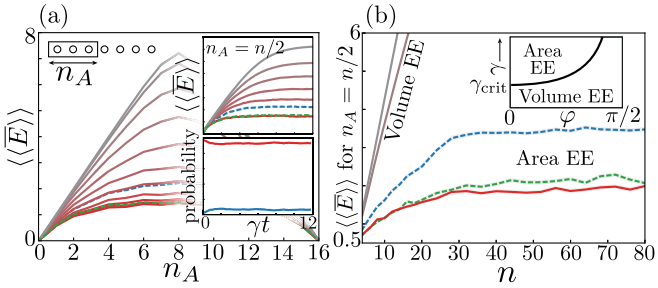

FIG. 3. EAEE for the open RBC. (a) EAEE profile in the long time limit for various unravelings. Solid lines denote homodyne unravelings with changing phase from $\varphi_j = 0$ (red) to $\varphi_j = \pi/2$ (gray) in increments of $\pi/20$, and dashed blue and green lines correspond to the number and EOQT measurements. Insets: Time evolution of EAEE for various unravelings and measurement choices of the EOQT. Here $m = n = 16, \chi = 128$. (b) Half-chain EAEE for larger systems (with $\chi = 512$). Depending on the homodyne phase, the ensembles display an area law at small φ_j and a volume law at $\varphi_j \approx \pi/2$. The EOQT method results in an area-law EAEE close to the homodyne unraveling with $\varphi_j = 0$, whereas the number unraveling leads to an area law with larger EAEE. The phase diagram is shown in the inset. For all data in this figure we used $\alpha/\gamma = 0.1$ $(\alpha = 1)$ and $N = 200$. The statistical error bars lie within the lines' thickness.

where $d\xi_j(t) = 2\sqrt{\gamma}\langle\sigma_j^z\rangle(t)\cos\varphi_j dt + dW_j(t)$ (see Sec. VI of the Supplementary Material [26] for more details). It has a unitary part, $\exp\{i\sin(\varphi_j)\sqrt{\gamma}\sigma_j^z d\xi_j(t)\}$, and a nonunitary part, $\exp\{\cos(\varphi_j)\sqrt{\gamma}\sigma_j^z d\xi_j(t)\}$. The unitary component can be absorbed into the coherent part of the evolution, as it leaves the ensemble of RBCs invariant. The nonunitary component can be reinterpreted as a stochastic propagator of a Markov process with an effective decoherence rate $\gamma_j^{\mathrm{eff}} = \gamma\cos^2\varphi_j$. Changing the unraveling at fixed γ by changing φ_j is thus equivalent to changing γ for a fixed unraveling. This equivalence is remarkable, as these two interpretations describe two profoundly different physical scenarios: The first refers to various representations of the solution of a single ME, while the second refers to particular solutions of various MEs. The latter has been studied extensively recently [12–23], and it is known that the conditional states can undergo a so-called measurement-induced phase transition from area-law to volume-law entanglement, depending on the coupling strength to the environment. In our case, this phase transition occurs as a function of the unraveling, e.g., parametrized by φ_j. Indeed, for $\varphi_j = \pi/2$ the QTs map to fully coherent RBC evolution, which generates entanglement that obeys a volume law. In the other limiting case, $\varphi_j = 0$ (and sufficiently large γ), the measurement backaction continuously leads to an effective projection onto product states, resulting in entanglement within the system that satisfies an area law. These two phases are separated by a critical point at $\gamma\cos^2\varphi_j = \gamma_{\mathrm{crit}}$. Thus, when $\gamma > \gamma_{\mathrm{crit}}$, the many-body

ME can be efficiently solved using MPS via QTs *if* an efficient unraveling is chosen. In Fig. 3 we show results of MPS simulations of various unravelings of the open RBC demonstrating that the EOQT method indeed finds efficiently computable unraveling.

In summary, we introduced a novel QT method to simulate the time evolution of a noisy quantum many-body system and showed that our method can enable an efficient classical simulation, where standard QT methods may fail. While in this Letter we focused on monitoring and optimizing each output channel separately, more general schemes, based on collective monitoring and optimization, can be developed [32]. Detailed performance comparisons with other techniques for open quantum many-body systems [33–44] are left for future work.

We thank P. Zoller and B. Kraus for stimulating discussions. This work is supported by a Discovery Grant from the Erwin Schrödinger Center for Quantum Science & Technology (ESQ), and an ERC Starting Grant (No. 101041435).

*hannes.pichler@uibk.ac.at

[1] J. Preskill, Quantum **2**, 79 (2018).
[2] S. R. White, Phys. Rev. Lett. **69**, 2863 (1992).
[3] G. Vidal, Phys. Rev. Lett. **91**, 147902 (2003).
[4] U. Schollwöck, Ann. Phys. (Amsterdam) **326**, 96 (2011).
[5] R. Dum, P. Zoller, and H. Ritsch, Phys. Rev. A **45**, 4879 (1992).
[6] J. Dalibard, Y. Castin, and K. Mølmer, Phys. Rev. Lett. **68**, 580 (1992).
[7] C. W. Gardiner, A. S. Parkins, and P. Zoller, Phys. Rev. A **46**, 4363 (1992).
[8] L. Tian and H. J. Carmichael, Phys. Rev. A **46**, R6801 (1992).
[9] Y. Castin, J. Dalibard, and K. Mølmer, AIP Conf. Proc. **275**, 143 (1993).
[10] F. Van Dorsselaer and G. Nienhuis, Eur. Phys. J. D **2**, 175 (1998).
[11] C. Gardiner and P. Zoller, *The Quantum World of Ultra-Cold Atoms and Light Book II: The Physics of Quantum-Optical Devices* (World Scientific Publishing Company, Singapore, 2015).
[12] Y. Li, X. Chen, and M. P. A. Fisher, Phys. Rev. B **98**, 205136 (2018).
[13] Y. Li, X. Chen, and M. P. A. Fisher, Phys. Rev. B **100**, 134306 (2019).
[14] B. Skinner, J. Ruhman, and A. Nahum, Phys. Rev. X **9**, 031009 (2019).
[15] A. Chan, R. M. Nandkishore, M. Pretko, and G. Smith, Phys. Rev. B **99**, 224307 (2019).
[16] M. J. Gullans and D. A. Huse, Phys. Rev. Lett. **125**, 070606 (2020).
[17] S. Choi, Y. Bao, X.-L. Qi, and E. Altman, Phys. Rev. Lett. **125**, 030505 (2020).
[18] Y. Bao, S. Choi, and E. Altman, Phys. Rev. B **101**, 104301 (2020).
[19] A. Zabalo, M. J. Gullans, J. H. Wilson, S. Gopalakrishnan, D. A. Huse, and J. H. Pixley, Phys. Rev. B **101**, 060301(R) (2020).
[20] M. Ippoliti, M. J. Gullans, S. Gopalakrishnan, D. A. Huse, and V. Khemani, Phys. Rev. X **11**, 011030 (2021).
[21] A. Zabalo, M. J. Gullans, J. H. Wilson, R. Vasseur, A. W. W. Ludwig, S. Gopalakrishnan, D. A. Huse, and J. H. Pixley, Phys. Rev. Lett. **128**, 050602 (2022).
[22] T. Botzung, S. Diehl, and M. Müller, Phys. Rev. B **104**, 184422 (2021).
[23] T. Müller, S. Diehl, and M. Buchhold, Phys. Rev. Lett. **128**, 010605 (2022).
[24] G. Lindblad, Commun. Math. Phys. **48**, 119 (1976).
[25] A. J. Daley, Adv. Phys. **63**, 77 (2014).
[26] See Supplemental Material at http://link.aps.org/supplemental/10.1103/PhysRevLett.128.243601 for more detail.
[27] Since the trajectories are by construction sampled according to Born's rule, all such strategies, including the adaptive time- and history-dependent ones, generate trajectories that provide valid solutions of the ME [see Section I of the Supplementary Materials (SM) for more detail].
[28] W. K. Wootters, Phys. Rev. Lett. **80**, 2245 (1998).
[29] S. Gharibian, Quantum Inf. Comput. **10**, 343 (2010).
[30] A. J. Daley, C. Kollath, U. Schollwöck, and G. Vidal, J. Stat. Mech. (2004) P04005.
[31] S. R. White and A. E. Feiguin, Phys. Rev. Lett. **93**, 076401 (2004).
[32] M. Holland, S. Marksteiner, P. Marte, and P. Zoller, Phys. Rev. Lett. **76**, 3683 (1996).
[33] L. Bonnes and A. M. Läuchli, arXiv:1411.4831.
[34] J. Cui, J. I. Cirac, and M. C. Bañuls, Phys. Rev. Lett. **114**, 220601 (2015).
[35] A. H. Werner, D. Jaschke, P. Silvi, M. Kliesch, T. Calarco, J. Eisert, and S. Montangero, Phys. Rev. Lett. **116**, 237201 (2016).
[36] J. Jin, A. Biella, O. Viyuela, L. Mazza, J. Keeling, R. Fazio, and D. Rossini, Phys. Rev. X **6**, 031011 (2016).
[37] C. D. White, M. Zaletel, R. S. K. Mong, and G. Refael, Phys. Rev. B **97**, 035127 (2018).
[38] A. Biella, J. Jin, O. Viyuela, C. Ciuti, R. Fazio, and D. Rossini, Phys. Rev. B **97**, 035103 (2018).
[39] F. Schwarz, I. Weymann, J. von Delft, and A. Weichselbaum, Phys. Rev. Lett. **121**, 137702 (2018).
[40] M. J. Hartmann and G. Carleo, Phys. Rev. Lett. **122**, 250502 (2019).
[41] F. Vicentini, A. Biella, N. Regnault, and C. Ciuti, Phys. Rev. Lett. **122**, 250503 (2019).
[42] N. Yoshioka and R. Hamazaki, Phys. Rev. B **99**, 214306 (2019).
[43] A. Nagy and V. Savona, Phys. Rev. Lett. **122**, 250501 (2019).
[44] H. Weimer, A. Kshetrimayum, and R. Orús, Rev. Mod. Phys. **93**, 015008 (2021).